Molecular Orbital Study of O_2^- Adsorbed on Titanium Ions on Oxide Supports

Kazuyuki Tatsumi,[†] **Masaru Shiotani,**[‡] **and Jack H. Freed***

Department of Chemistry, Baker Laboratory, Cornell University, Ithaca, New York 14853 *(Received: November 9, 1982; In Final Form: March 3, 1983)*

An extended Hückel analysis of O_2^- adsorbed on Ti ions on oxide supports is presented. The potential energy surface is obtained for deformations between the two limiting structures of the O_2^- parallel to the surface and end-on. A stable conformation is found for the parallel form, consistent with recent ESR results, and there is a maximum in energy between the two limiting structures. The observed near equality of the ESR hyperfine splittings of the two O atoms is found to be consistent with a small tilting of the O_2 axis from the parallel conformation (i.e., <10°). A low barrier for planar rotation of O_2^- about the axis perpendicular to the surface is also found, consistent with the small activation energy obtained from ESR line-shape analysis. The predicted **g**-tensor components allow unambiguous assignment of the ESR results, and a discussion is given on how variations in the extended Hückel parameters improve agreement with experiment.

Introduction

Transition-metal complexes of the superoxide O_2^- and the peroxide O_2^{2-} are of both chemical and biochemical interest.[1] We have previously reported on an ESR study of O_2^- adsorbed on Ti ions on porous Vycor glass (PVG).[2] The careful analysis of the temperature-dependent ESR line shapes led us to the conclusion that the motion of O_2^- is highly anisotropic, consisting essentially of planar rotation about the axis perpendicular to the molecular axis of O_2^- and parallel to the normal to the surface. In that paper, we briefly mentioned that the observed ESR parameters were consistent with the theoretical estimates obtained by extended Hückel[3] molecular orbital calculations. We wish to present here an account of the molecular orbital analysis. Our prime concern is in understanding the nature of bonding between O_2^- and Ti ions supported on PVG and the consequences thereof on the geometry and rotational barriers of O_2^-. We also consider how the **g**-tensor components compare with the experimental ones.

Geometry and Electronic Property of Dioxygen on Ti Ion

Model Ti Active Site. The local environment of Ti ions on porous Vycor glass (major composition: SiO_2 (97%)[4]) is not yet known. A reasonable assumption is that a Ti atom is surrounded by oxygen atoms of the silica at the surface leaving one coordination site open, which will allow Ti to interact with O_2. This octahedral arrangement of the oxygens around the Ti atom on the surface is consistent with the octahedral array of the TiO_2 system, the SiO_2 system being tetrahedral. The oxidation state of the Ti ion before the introduction of O_2 was suggested to be 3+ according to the experimental evidence.[2] Thus the adsorption of O_2 on the Ti site may be expressed formally as (Ti^{3+}–O_2) or (Ti^{4+}–O_2^-). Structure 1 is our model of the

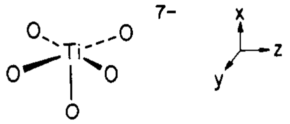

1

active Ti site used for the calculations. Five oxygen atoms are coordinated to Ti, four of which (O_{eq}) sit in the *yz* plane and one (O_{ax}) is below the Ti. Following the usual convention, the 7− charge is put on the TiO_5 fragment in order to create a 3+ oxidation state of Ti, corresponding to the d^1 electronic configuration. When Ti is in the *yz* plane, all the Ti–O distances are set at 1.944 Å.[5]

Alternative Structures of Dioxygen Coordinations. The bonding picture of O_2 to the TiO_5^{7-} fragment spans the range of geometrical possibilities from the side-on or η^2 coordination 2, with C_{2v} symmetry, through the bent or

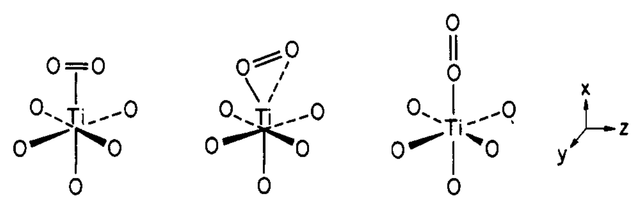

C_{2v} C_s C_{4v}

2 **3** **4**

kinked structure 3, with C_s symmetry, to the linear or end-on coordination 4, with C_{4v} symmetry. In the limiting geometry 2, the molecular axis of O_2 lies parallel to the *yz* plane, the two Ti–O bond distances being equal. The other limit 4 contains the linear TiO_2 arrangement which is on the *x* axis. Considering the approximate nature of the extended Hückel method, it is not worthwhile to construct a full potential energy surface for the O_2 deformation. Instead we choose a model deformation coordinate in which the x–Ti–O^1 angle α and the Ti–O^1–O^2 angle β are both varied (cf. Figure 1). Geometries 2 and 4 correspond to $\alpha = 20.8°$, $\beta = 69.2°$ and to $\alpha = 0°$, $\beta = 180°$, respectively (with θ, the tilt angle given by $\theta = \alpha + \beta - 90°$). Also, the position of the Ti ion, i.e., either in the $(O_{eq})_4$ plane or out

† Present address: Department of Macromolecular Science, Faculty of Science, Osaka University, Toyonaka, Osaka 560, Japan.

‡ Present address: Faculty of Engineering, Hokkaido University, Sapporo 060, Japan.

(1) See the following reviews: (a) I. B. Afanas'ev, *Russ. Chem. Rev. (Engl. Transl.)*, **48**, 527 (1980); (b) J. C. Vedrine, *Spec. Colloq. Ampere, Abstr. Lect. Posters, 4th, 1979*, 29 (1979); (c) J. H. Lunsford, *Catal. Rev.*, 8, 135 (1973); (d) J. Valentine, *Chem. Rev.*, **73**, 235 (1973); (e) G. Henrici-Olivé and S. Olivé, *Angew. Chem., Int. Ed. Engl.*, **13**, 29 (1974); (f) F. Basolo, B. M. Hoffman, and J. A. Ibers, *Acc. Chem. Res.*, **8**, 384 (1975); (g) L. Vaska, *ibid.*, **9**, 175 (1976); (h) G. McLendon and A. E. Martell, *Coord. Chem. Rev.*, **19**, 1 (1976).

(2) M. Shiotani, G. Moro, and J. H. Freed, *J. Chem. Phys.*, **74**, 2616 (1981).

(3) R. Hoffmann, *J. Chem. Phys.*, **39**, 1397 (1963).

(4) General information on Vycor brand porous glass No. 7930, Corning Glass Co., 1979.

(5) J. H. Horsley, *J. Am. Chem. Soc.*, **101**, 2870 (1979).

0022-3654/83/2087-3425$01.50/0

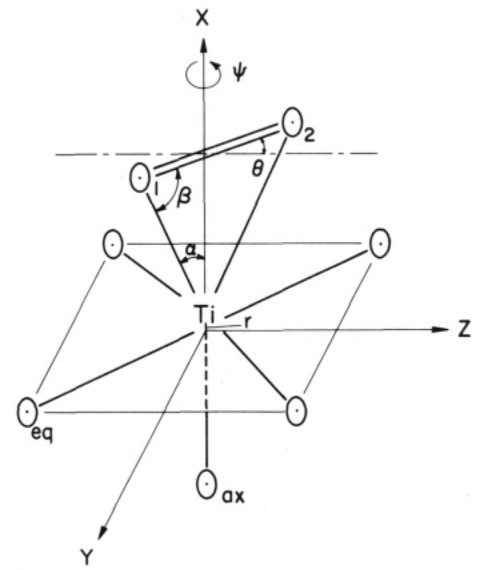

Figure 1. Model deformation coordinate of O_2 in $Ti(O_5)O_2^{7-}$. The out-of-plane displacement of Ti, r, and the angles α, β, (or θ) are varied simultaneously from the side-on to end-on geometries. Fixed are O^1–O^2 = 1.30 Å, Ti–O_{ax} = 1.944 Å, Ti–O_{eq} = 1.944 Å, and Ti–O^1 = 1.83 Å.

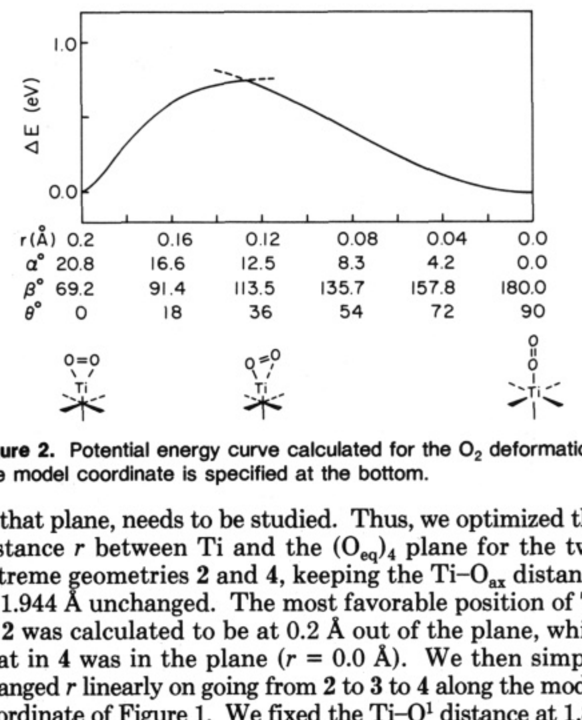

Figure 2. Potential energy curve calculated for the O_2 deformation. The model coordinate is specified at the bottom.

of that plane, needs to be studied. Thus, we optimized the distance r between Ti and the $(O_{eq})_4$ plane for the two extreme geometries **2** and **4**, keeping the Ti–O_{ax} distance of 1.944 Å unchanged. The most favorable position of Ti in **2** was calculated to be at 0.2 Å out of the plane, while that in **4** was in the plane (r = 0.0 Å). We then simply changed r linearly on going from **2** to **3** to **4** along the model coordinate of Figure 1. We fixed the Ti–O^1 distance at 1.83 Å,[6] the O^1–O^2 length at 1.30 Å, and the staggered orientation of O_2 with respect to $(O_{ea})_4$.

Figure 2 gives the potential energy curve that we calculated for the model coordinate, where the ground doublet electronic configuration is assumed. The curve yields a stable conformation for geometry **2**. The energy goes up as O_2 bends, reaching a maximum at around $\alpha = 15°$, and further deformation stabilizes the molecule again. Another potential minimum comes at $\alpha = 0°$, $\beta = 180°$, **4**. These features of the potential surface accord well with a more general energy diagram discussed for coordination modes of diatomic molecules in transition-metal complexes.[7] Although Figure 2 by itself does not show which structure

(6) R. Guilard, M. Fontesse, P. Fournari, C. Lecomte, and J. Protas, *J. Chem. Soc., Chem. Commun.*, 161 (1976).
(7) R. Hoffmann, M. M.-L. Chen, and D. L. Thorn, *Inorg. Chem.*, **16**, 503 (1977).

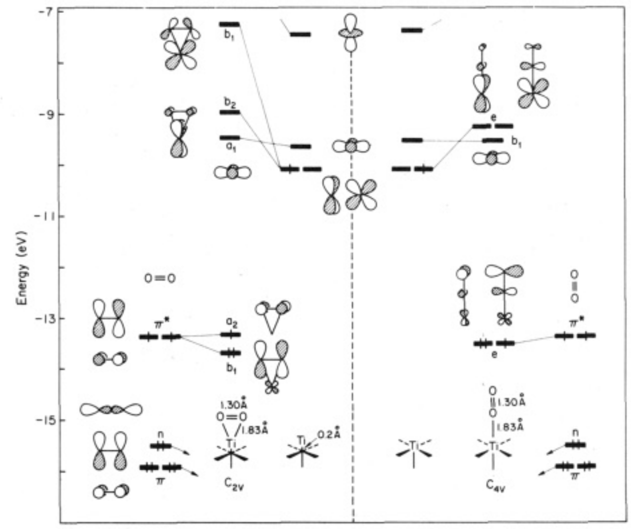

Figure 3. Interaction diagrams for O_2 and the $Ti(O_5)^{7-}$ fragment for the side-on geometry (to the left of the dashed line) and the end-on geometry (to the right). At the middle, the $Ti(O_5)^{7-}$ fragment for either of the two geometries carries four low-lying Ti d orbitals, while the high-lying yz orbital is not shown. The symmetry assignment of the orbitals is based on the standard coordinate system which retains the main symmetry axis where the fourfold axis of $Ti(O_5)^{7-}$ used to be, though our choice of coordinate differs from this.

2 or **4** is the best conformation, we should note here that the ESR experiment rules out the possibility that **4** is the one observed, as will be discussed in a later section.

There are a number of O_2 complexes of the early transition metals. Several structures are available, all η^2 and d^0 if O_2 is regarded as peroxide O_2^{2-}. Among these include $MoOF_4(O_2)^{2-}$,[8a] $[Ti(O_2)(dipic)O]_2O^{2-}$,[8b] $TiF_2(dipic)(O_2)^{2-}$ and $Ti(H_2O)_2(dipic)(O_2)$,[8c] $VO(H_2O)(dipic)(O_2)^-$,[8d] Ti(octaethylporphyrin)O_2,[8e] and Mo(tetraphenylporphyrin)$(O_2)_2$.[8f] Note that $Ti(O_2)(O)_5^{7-}$ may be regarded as the Ti(IV) d^0 electronic configuration with a single negative charge on O_2. Some O_2 complexes have kinked structures **3**, but all of them carry five to six electrons at the metal centers, while O_2 assumes a single negative charge.[9]

Interaction Diagram. The molecular orbitals of the two extreme geometries **2** and **4** are constructed in Figure 3. In the middle of the figure, there are four d-block orbitals of each Ti fragment, r = 0.2 Å and r = 0.0 Å. The yz orbital is high above in energy due to the strong ligand field of $(O_{eq})_4$, and is not shown. For r = 0.0 Å, there is a set of three low-lying d orbitals, y^2–z^2 (b_1), and xz, xy (e), while x^2 (a_1) is located at a somewhat higher energy. The small out-of-plane displacement of Ti (r = 0.2 Å) affects these orbitals only slightly. Note that the symmetry assignment of the orbitals is based on the standard coordinate system in which the principal symmetry axis is the fourfold axis of the $(TiO_5)^{7-}$, although we label our axes differently. At both ends, O_2 carries doubly occupied n and π orbitals as well as half-occupied π^* orbitals.

The left half of Figure 3 shows the interaction diagram for the side-on geometry. x^2 and xy are pushed up by

(8) (a) D. Grandjean and R. Weiss, *Bull. Soc. Chim. Fr.*, 3044 (1967); (b) D. Schwarzenbach, *Inorg. Chem.*, **9**, 2391 (1970); (c) D. Schwartzenbach, *Helv. Chim. Acta*, **55**, 2990 (1972); (d) R. E. Drew and F. W. B. Einstein, *Inorg. Chem.*, **12**, 829 (1973); (e) see ref 6; (f) B. Chevrier, T. Diebold, and R. Weiss, *Inorg. Chim. Acta*, **19**, L57 (1976).
(9) (a) J. P. Collman, R. R. Gagne, C. A. Reed, W. T. Robinson, and G. A. Rodley, *Proc. Natl. Acad. Sci. U.S.A.*, **71**, 1326 (1974); J. P. Collman, R. R. Gagne, C. A. Reed, T. R. Halbert, G. Lang, and W. T. Robinson, *J. Am. Chem. Soc.*, **97**, 1427 (1975); (b) L. D. Brown, and K. N. Raymond, *Inorg. Chem.*, **14**, 2595 (1975); (c) S. K. Cheung, C. J. Grimes, J. Wong, and C. A. Reed, *J. Am. Chem. Soc.*, **98**, 5028 (1976).

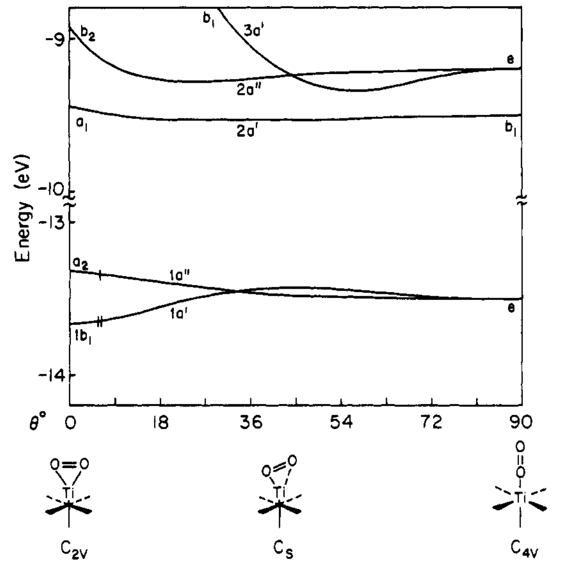

Figure 4. Walsh diagram for O_2 deformation. The model coordinate is the same as the one specified in detail at the bottom of Figure 2.

interactions with O_2 $\pi_\perp$ (and n) and $\pi_\parallel$, respectively, by a different amount (see **5**). The most important feature

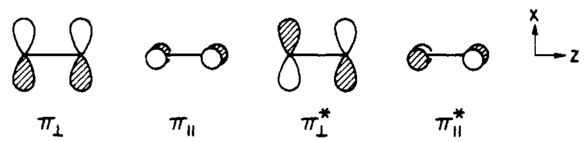

5

of the level scheme is that the originally degenerate O_2 π^* orbitals split slightly into two levels. $\pi_\perp^*$ (b_1) moves down in energy by an interaction with xz. $\pi_\parallel^*$ (a_2) finds a symmetry match with Ti yz, but the weak π-type interaction leaves $\pi_\parallel^*$ nearly at its original energy level. Although the a_2–b_1 level splitting is not great, an unpaired electron most likely resides in the a_2 orbital in the ground state. At the right half of Figure 3, molecular orbitals of the linear structure are constructed. The O_2 π^* orbitals interact with xz and xy by an equal amount. The orbital degeneracy at the highest occupied energy region is not removed, so that three electrons should go into the e orbitals.

Walsh Diagram. Figure 4 shows how the five valence orbitals of $(TiO_5–O_2)^{7-}$ change their energies along the model deformation coordinate. As α decreases and β increases, the b_1 ($\pi_\perp^* + xz$) orbital is first destabilized and then comes down to become one of the e orbitals of the geometry **4**. Since the evolution of b_1 was analyzed in detail by Hoffmann, Chen, and Thorn,[7] we avoid duplication here. We just note that their discussion was primarily for the $ML_4(XY)$ system while our model compound $(TiO_5–O_2)^{7-}$ has an extra-"ligand" O_{ax} at a position opposite to O_2. The behavior of the b_1 level is the major factor causing the potential maximum present at the kinked structure in Figure 2. a_2 (a'' in C_s symmetry) is gradually stabilized, crosses the ascending b_1 (a' in C_s) level, and eventually merges with a' again at the linear geometry. The growing $\pi_\parallel^*$–xy interaction is the reason for the stabilization of a_2 on going from **2** to **3** to **4**.

Comparison between the Calculated and Experimental Results

Half-Occupied Molecular Orbital. The potential energy curve in Figure 2 shows that the energetically favored orientation of O_2 on Ti ion is either **2** or **4**. The ESR experiments[2] however, clearly exclude the possibility of the

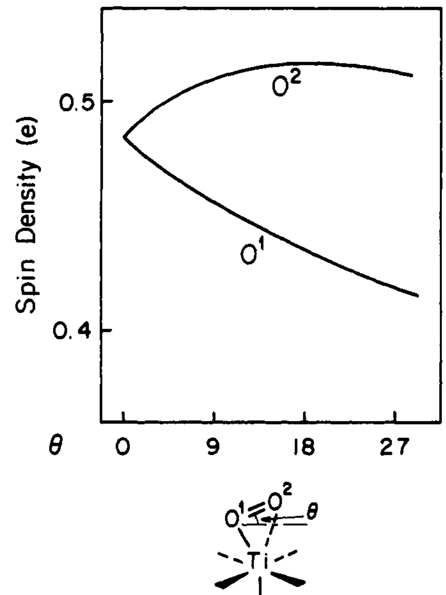

Figure 5. Variation of spin distribution at O_2 calculated as a function of O_2 deformation.

end-on geometry **4** as the O_2^- species which is observed. At 4 K three **g**-tensor components were measured for $^{16}O_2^-$: $g_1 = 2.0025$, $g_2 = 2.0092$, and $g_3 = 2.0271$. Furthermore, the observed hyperfine splitting (hfs) of ^{17}O is almost axially symmetric; $A_\parallel = 74.8$ G, $A_\parallel' = 80.3$ G, and $A_\perp \leq 3$ G. The former two components can be seen as a doublet at the $M_I = \pm5/2$ and $\pm3/2$ bands, the center of which is located at g_1. These observations are explicable when we assume the unpaired electron resides in the a_2 orbital of **2**, which consists mainly of O_2 $\pi_\parallel^*$. If the half-occupied molecular orbital is one of the e orbitals of the geometry **4**, then, just as in a free O_2^- molecule, the **g** tensor should be $g_{xx} = g_{yy} = 0$ and $g_{zz} = 4$,[10] but a Renner–Teller distortion[11] of this structure could be expected (i.e., a value of $\beta < 180°$ due to vibronic coupling). If such a conformation exists, it might not be detectable by standard ESR experiments, possibly due to excessive line broadening.

Next let us consider the nonequivalence of the two oxygen nuclei. Using ^{17}O-enriched O_2, we observed two different parallel components of ^{17}O in $(^{17}O–^{18}O)^-$.[2] This suggests a tilting of the internuclear axis of O_2^- from the surface so that one oxygen atom is closer to the Ti^{4+} than the other. On the other hand, the analysis of the temperature-dependent ESR line shape showed that the degree of the tilting θ should not be so large, probably less than 10°.

The observation of the two ^{17}O hfs allows us to estimate the spin densities on the O_2^- ion. $A_\parallel = 74.8$ G and $A_\parallel' = 80.3$ G corresponds to $0.49e$ and $0.52e$, respectively. In Figure 5 the spin distribution at O_2 calculated by the extended Hückel method is shown as a function of θ, α, or β. Although the calculated values themselves do not accord very well with the experimental ones, the following two interesting trends may be seen. First, the oxygen atom O^1, which is closer to Ti, assumes smaller spin density than the distant one O^2. Therefore, the observed hfs $A_\parallel$ can be attributed to O^1 and $A_\parallel'$ to O^2. Second, the difference in spin densities at O^1 and O^2 becomes larger as θ increases as expected. The observed spin polarization is rather small, amounting to only $0.03e$.[12] This is consistent with

(10) W. Känzig and M. H. Cohen, *Phys. Rev. Lett.*, **3**, 509 (1959).
(11) G. Herzberg, "Electronic Spectra of Polyatomic Molecules", Van Nostrand, New York, 1966, pp 26–37.

the calculated polarization only when the tilting of O_2 is very small, i.e., $\theta < 9°$. Remember that the ESR line-shape study also indicates at most a slight tilting.

The energetically most favorable geometry (consistent with the ESR results) was calculated to be the one in which O_2 stays parallel to the $(O_{eq})_4$ plane of our model. In this geometry the two oxygen atoms ought to be equivalent, while the ESR study shows nonequivalence of O_2 though the difference is very small. In the real system of O_2^- adsorbed on Ti ion supported by PVG, there may exist some irregularity of the surface, which will result in such a small deviation from the precise side-on structure, or else the extended Hückel method is not able to predict such a small deviation. Regardless of the minor tilting of O_2, however, it is safe to say that an unpaired electron resides in the a′ (a_2 in the C_{2v} symmetry), i.e., in the O_2 $\pi_{\parallel}^*$ orbital.[13]

Rotational Barrier of O_2. We have reported that the molecular motion of O_2^- on the Ti–PVG surface is highly anisotropic, consisting essentially of planar rotation about the axis perpendicular to the internuclear axis of O_2^- and parallel to the surface. This conclusion was derived from the detailed analysis of the temperature-dependent ESR line shape of $^{16}O_2^-$. The rotational correlation time for the planar motion, $\tau_{R_{\parallel}}$ (cf. ref 2), is essentially independent of the rotational diffusion model used above 100 K and decreased exponentially as a function of $1/T$(K). A rather small activation energy of 0.5 kcal/mol (0.022 eV) was found for the rotational diffusion of O_2^- from the linear relation between ln $\tau_{R_{\parallel}}$ and $1/T$ above 100 K.

We computed rotational barriers of O_2 in our model $(TiO_5–O_2)^{7-}$ by the extended Hückel method. O_2 was rotated about the x axis going from the staggered conformation to the eclipsed one for geometries with given tilt angle θ. Since the tilting is likely to be less than 10°, as discussed in the previous section, we give the computed barriers only for geometries of θ = 0°, 9°, and 18°. These are 0.062, 0.045, and 0.027 eV, respectively, where the energy maximum comes at the eclipsed conformation while the minimum is at the staggered one. All are fairly small, being consistent with the experimental observation. It should be noted here that the above discussion refers to a simple rigid rotation of O_2 with θ being kept constant. If wobble motion is taken into account, apparent barriers might get smaller.

*Principal Values of **g** Tensor.* The fully anisotropic **g**-tensor components g_1 = 2.0025, g_2 = 2.0092, and g_3 = 2.0271 were observed experimentally for $^{16}O_2^-$ at 4.2 K, the lowest temperature of our measurement.[2] Although the ESR spectrum at 4.2 K is not precisely at the rigid limit, we believe that the **g**-tensor components at 4.2 K should be very close to it.[2] The principal values of the **g** tensor were analyzed on the basis of the expressions originally given by Känzig and Cohen[10] and correlated with the molecular form: $g_{xx} = g_2$, $g_{yy} = g_1$, and $g_{zz} = g_3$. This analysis is consistent with the experimental evidence which shows the ^{17}O hf tensor as axially symmetric and the parallel component of the hf splitting at the g_{yy} component.[2]

The expressions for the **g** tensor given by Känzig and Cohen are based on simple crystal field theory in which, e.g., the central ion is regarded as a point charge. The inclusion of bonding such as by the extended Hückel method would be equivalent to ligand-field theory, so predictions of the **g**-tensor components for our system would provide further insights to the molecular orbital structure. We therefore computed the principal values of the **g** tensor based on the extended Hückel molecular orbitals, and compared the results with the experimental ones.

The general expressions for the components of the **g** tensor have been obtained from the standard perturbation theory:[14]

$$g_{\alpha\beta} = 2.0023 - 2\sum_{n}\sum_{k,j}\{\langle\psi_0|\xi_k\hat{L}_{\alpha k}\delta_k|\psi_n\rangle\langle\psi_n|\xi_k\hat{L}_{\alpha k}\delta_k|\psi_0\rangle/(\epsilon_n - \epsilon_0)\} \quad (1)$$

TABLE I: Observed and Calculated g-Tensor Components for O_2^-/Ti-Vycor

θ, deg	g_{zz}	g_{yy}	g_{xx}
Side-On Bent Geometry			
0	2.0718	2.0028	2.0130
9	2.0925	2.0028	2.0149
18	2.1519	2.0031	2.0274
27	2.4158	2.0035	2.1229
Side-On Geometry[a]			
H_{ii}(Ti,3d), eV	g_{zz}	g_{yy}	g_{xx}
−12.11	2.0718	2.0028	2.0130
−13.11	2.0604	2.0028	2.0129
−14.11	2.0517	2.0028	2.0127
−15.11	2.0452	2.0028	2.0126
Side-On Geometry[b]			
Ti–O, Å	g_{zz}	g_{yy}	g_{xx}
1.83	2.0718	2.0028	2.0130
1.64	2.0595	2.0032	2.0122
1.46	2.0489	2.0038	2.0109
1.29	2.0387	2.0042	2.0092
obsd	2.0271	2.0025	2.0092

[a] Ti–O = 1.83 Å. [b] H_{ii}(Ti,3d) = −12.11 eV.

TABLE II: Parameters Used in Extended Hückel Calculations[a]

orbital	H_{ii}, eV	ζ_1	ζ_2	C_1[b]	C_2[b]
Ti 3d	−12.110[c]	4.550	1.40	0.4206	0.7839
4s	−9.790[c]	1.075			
4p	−6.027[c]	0.675			
O 2s	−32.30	2.275			
2p	−14.80	2.275			

[a] The basis set used for Ti consisted of single Slater orbitals for 4s and 4p, and a contracted linear combination of two Slater orbitals for 3d. The exponents were taken from the work of Richardson et al.[17] The parameters for O are standard ones. [b] Contraction coefficients used in the double-ζ expansion, where the ζ are the exponents. [c] A charge iterative calculation was carried out on the $(TiO_5)^{7-}$ fragment assuming a quadratic charge dependence for the H_{ii} of Ti. This is the normal procedure utilized.[7] Ti sits in the $(O_{eq})_4$ plane and the Ti–O distances are 0.944 Å.

(12) We may note here that the calculated spin density in the Ti d orbital is almost zero (i.e., ρ_{Ti} = 0.0001) for the side-on geometry 2, since the spin density is essentially located in the π^* orbitals of the two oxygens (i.e., $\sum\rho_O$ = 0.97). As the bend angle θ increases, the spin density in the Ti increases slightly (e.g., ρ_{Ti} = 0.02 and $\sum\rho_O$ = 0.93 for θ = 27°).

(13) We also performed calculations for the geometry in which the internuclear axis of O_2 is parallel to the O_4 plane, but the center of the O═O bond is shifted with respect to the Ti atom. For a 2:1 ratio of the O atom distances from the x axis, the displacement of Ti ion giving the lowest energy is again r = 0.2 Å, but the computed total energy is 0.28 eV higher than geometry 2. Moreover, the spin densities are 0.45 and 0.52 for the oxygen closer to and further from the Ti ion, respectively. It also leads to a significant increase in g_{zz} over 2 (2.0918) with g_{yy} and g_{xx} virtually unchanged (2.0027 and 2.0137, respectively). Our analysis does not rule out *small* shifts of the O═O center with respect to the Ti atom.

(14) A. Carrington and A. D. McLachlan, "Introduction to Magnetic Resonance", Harper and Row, New York, 1967; a recent application of the theory to $[CrOCl_4]^-$, is given by K. K. Sunil, J. F. Harrison, and M. T. Rogers, *J. Chem. Phys.*, 76, 3078 (1982).

where ψ_0 and ϵ_0 denote the wave function and energy of the half-occupied orbital, ψ_n and ϵ_n are those of unoccupied and doubly occupied orbitals, and ξ_k refers to the one-electron spin–orbit coupling of atomic orbital k. The spin–orbit coupling parameters used are ξ(Ti,3d) = 0.05 eV[15a] and $\xi(O^-,2p)$ = 0.014 eV,[15b] while the contribution from Ti 4p is ignored. The sum runs over all pairs of k and j. The symbol δ_k is zero unless the $\hat{L}_{\alpha k}$, α-th component of orbital angular momentum, acts on the same atomic orbital as k.

First the **g**-tensor components were calculated for the side-on geometry, **2**, and are g_{zz} = 2.0718, g_{yy} = 2.0028, and g_{xx} = 2.0130. These are compared with our ESR results in Table I. (The parameters used in the extended Hückel calculations are given in Table II.) The computed g_{yy} and g_{xx} values agree rather well with those experimentally observed, while the g_{zz} value is somewhat too large. The calculated trend, $g_{zz} > g_{xx} > g_{yy}$, however, confirms our assignment of the observed three g components, g_1, g_2, and g_3. The contribution to g_{zz} comes mostly from the excitation $1b_1 \rightarrow a_2$ (cf. Figure 3) with the calculated excitation energy of 0.3592 eV. On taking this single contribution into account, we get a value of 2.0704 for g_{zz}. Naturally the g_{zz} value is very sensitive to the $1b_1 \rightarrow a_2$ excitation energy obtained. The extended Hückel method may underestimate the $1b_1$–a_2 separation. The magnitude of g_{yy} is determined by several excitations from or to the a_2 molecular orbital, where O_{ax} and O_{eq} atomic orbital components in a_2 mainly participate in g_{yy}. The O_2 portion does not contribute to g_{yy} due to a symmetry restriction, if we use expression 1. On the other hand, most of the contribution to g_{xx} is from the excitation $O_2\ \sigma \rightarrow a_2$, the former of which spreads over several molecular orbitals ranging from −15.7 to −16.4 eV.

Next calculated are **g** tensors of bent structures at θ = 9°, 18°, and 27°, which are summarized in Table I together with those of the side-on geometry, θ = 0°. As O_2 is bent from θ = 0° to θ = 27°, the three **g**-tensor components all become much larger, thus deviating more from the ESR results. The substantial increment of g_{zz} can be attributed to a decrease in the $1b_1(1a')$–$a_2(1a'')$ energy separation as is seen in the Walsh diagram of Figure 4. This calculated trend is strongly suggestive of little or no bending of O_2 from the side-on geometry.

Kasai has given an expression for the **g**-tensor components of O_2^- adsorbed on γ- and X-ray irradiated zeolites,[16] which is essentially the same as that of Känzig and Cohen.[10] The O_2^- $\pi_\parallel^*$–$\pi_\perp^*$ splitting is denoted as δ and the $\pi_\parallel^*$–σ separation is denoted as Δ. There is no inclusion of the orbitals of the parent metal ion, to which the O_2^- is chemically bonded. The extended Hückel results can be used to obtain values for δ and Δ rather than to regard them as empirical parameters. However, since the $O_2\ \sigma$ orbital spreads over several molecular orbitals of Ti-$(O_5)O_2^{7-}$, we had to regard the molecular orbital with the largest $O_2\ \sigma$ character as the primary $O_2\ \sigma$. Its energy is −16.4366 eV. We obtained the values g_{zz} = 2.0802, g_{yy} = 2.0010, and g_{xx} = 2.0096 for the end-on structure, which are similar to, but not the same as, the values in Table I.

Our primary objective in calculating the **g** tensors was to see whether we could predict the observed order of magnitude of g_{xx}, g_{yy}, and g_{zz} using the "standard" extended Hückel and geometrical parameters. Thus, we did not undertake a large effort to improve the fit of the calculated **g**-tensor components to the observed ones by "adjusting" the geometrical and extended Hückel parameters. Let us briefly examine how the changes in these parameters do affect the calculated g values of the side-on structure, θ = 0°. We mentioned that the small $1b_1$–a_2 splitting is the reason for too large a g_{zz} value. If the parameters are varied so as to enlarge the energy separation, one may expect to get a smaller g_{zz}, thus better agreement with the experiment. The enhancement of the splitting should be achieved when the $O_2\ \pi_\perp^*$–Ti xz interaction is increased. There are two distinct ways of doing this. One is to lower the Ti orbital energy and the other is to shorten the Ti–O_2 separation. We varied either the Ti 3d energy from the original value of −12.11 to −15.11 eV, or the Ti–O distances from 1.83 to 1.29 Å. The calculated g_{zz} and the other g components are given in Table I. In fact, g_{zz} becomes smaller as the d energy is lowered and as the Ti–O distance is shortened. An improvement of g_{xx} is also attained. The change in Ti d energy does not affect g_{yy}, while shortening the Ti–O bond results in a larger g_{yy} value.

Summary

Our extended Hückel molecular orbital calculations for O_2^- adsorbed on Ti ions supported on PVG, which were based on standard parameters and geometries, leads to predictions in reasonable agreement with ESR results, and they help to confirm their interpretation. In particular, we find a stable conformation for end-on geometry of O_2^- and a very low activation barrier for rotation of O_2^- about an axis perpendicular to the surface. The ESR results do, however, indicate a small tilting of the O_2 axis from the predicted parallel conformation. The calculated **g** tensor confirms the previous assignment of the experimental values, but g_{zz} is rather larger than experiment. Its magnitude can be brought closer to the experimental one by (arbitrarily) lowering the Ti orbital energy used or by shortening the Ti–O separation, but such procedures are not necessarily justified. Finally, although an end-on geometry for O_2^- is not ruled out by our analysis, it would not yield conventional ESR spectra at $g \approx 2$.

Acknowledgment. K.T. is grateful to Professor Roald Hoffmann for stimulating discussions. This research was supported by Grant no. DE-AC02-80 ER04991 from the Office of Basic Energy Sciences of the DOE and by the Cornell Material Science Center (NSF).

Registry No. O_2, 11062-77-4; Ti, 7440-32-6; silica (vitreous), 60676-86-0.

(15) (a) The spin–orbit coupling constant for $Ti^{4+}(3s^23p^6)$ is not known, but should be larger than that for $Ti^{3+}(3d^1)$. For the latter, $\xi(Ti^{3+}(3d^1))$ = 154 cm^{-1} (0.019 eV) has been reported. See, for example, A. Abragam and B. Bleaney, "Electron Paramagnetic Resonance", Oxford Press, Oxford, 1970, p 378. Note that the calculated **g**-tensor component was essentially unchanged when ξ(Ti) = 0.025 eV was used due to the small spin density on the Ti atom (cf. ref 12). (b) see ref 16.

(16) P. H. Kasai, *J. Chem. Phys.*, **43**, 3322 (1965); P. H. Kasai and R. J. Bishop, *ACS Monogr.*, **No.** 171, 350 (1976).

(17) J. W. Richardson, W. C. Nieuwpoort, R. R. Powell, and W. E. Edgell, *J. Chem. Phys.*, **36**, 1057 (1962).